Chapter 20
Numerical Solution of the Tri-harmonic Kirchhoff Plate Equation Resulting from a Strain Gradient Theory

Christian Liebold & Belal M. Dawwas

Abstract A second gradient continuum theory is formulated based on second gradients of displacements. For a reduction of additional material parameters, the modified strain gradient model is used and a partial differential equation of rank six is developed using the Kirchhoff plate assumptions. The solutions of the governing tri-harmonic plate bending equation incoorperate size-effects. Balance equations are presented and higher-order stress-strain relations are derived. In order to account for second gradients of displacements, which manifest themselves in the higher-order terms of a strain energy density, a C^1–continuous displacement field is preferable. So-called Hermite finite element formulations allow for merging gradients between elements and are used to achieve global C^1–continuity of the solution. Element stiffness matrices as well as the global stiffness matrix are developed for a lexicographical order of nodes and for equidistantly distributed elements. The convergence, the C^1–continuity, and the size effect are demonstrated.

Keywords: Second gradient elasticity · Size-effect · Hermite finite elements · Continuum mechanics · Computational mechanics · Tri-harmonic equation

20.1 Introduction

Materials with intrinsic micro or nano-structure may show size-dependent material behavior, which is reflected, *e. g.*, in a stiffer elastic response to external forces, when the size of the material body is reduced. A quantitative understanding of a size effect is of great importance when modeling Micro- and Nano-Electro-Mechanical Systems (MEMS/NEMS). Driven by the miniaturization as an improvement of the

Christian Liebold & Belal M. Dawwas
Technische Universität Berlin, Chair of Continuum Mechanics and Constitutive Theory, Einsteinufer 5, 10587 Berlin, Germany,
e-mail: christian.liebold@mail.de, belal.m.dawwas@campus.tu-berlin.de

B. E. Abali et al. (eds.), *New Achievements in Continuum Mechanics and Thermodynamics*, Advanced Structured Materials 108,
https://doi.org/10.1007/978-3-030-13307-8_20

performance of MEMS, the requirement of reliability in simulation techniques increases. Experimental validation for size effects is given in, *e. g.*, Cuenot et al (2004); Lam et al (2003); Li et al (2010); McFarland and Colton (2005). Materials which are modeled this way are referred to as "non-simple materials of the gradient type". This is accurate, for example, for polymers at a small scale, or even fibre-reinforced materials (Giorgio et al, 2018). In Sect. 20.2 the present work deals with the KIRCHHOFF plate assumptions as well as the *Modified Strain Gradient theory* (MSG) developed by, *e. g.*, Mindlin and Tiersten (1962); Toupin (1962), since conventional continuum theories based on the CAUCHY continuum are not able to predict size effects. As a result, a tri-harmonic partial differential equation for plates is derived. Their solution for a boundary value problem of a rectangular plate under a uniform load is numerically investigated in Sect. 20.3. The application of conventional Finite Element (FE) strategies may lead to inaccurate results, if finite element formulations are used, which only fulfill global C^0–continuity. The scope of this work is, to develop a FE formulation based on HERMITE polynomials in order to account for C^1–continuity of the solution for the tri-harmonic plate equation.

20.2 The Tri-harmonic Plate Equation

20.2.1 Modified Strain Gradient Theory

The present work is based on one of the three reduced forms of the strain gradient energy density for small deformations, as postulated by Mindlin and Tiersten (1962). Because of the later on modification of this theory by an introduction of a rotational degree of freedom, the resulting theory is addressed as *modified strain gradient theory* here, different to the common name *modified (indeterminate) couple stress theory* frequently to be found in the litarature (Eremeyev and dell'Isola, 2018). The fact, that the rotational degree of freedom in the kinematical description of the continuum is replaced by a second gradient of displacement (valid for solids under small translational and rotational deformation only), supports the naming here. In what follows, the EINSTEIN summation convention is used on repeated indices. Spatial partial derivatives in the Cartesian coordinate system are denoted by comma-separated indices. MINDLIN's second form of a linear isotropic strain energy density originally reads:

$$\begin{aligned} u^{\mathrm{SG}} &= \alpha_1 \varepsilon_{ij}\varepsilon_{ij} + \alpha_2 \varepsilon_{kk}\varepsilon_{mm} \\ &\quad + \beta_1 \eta_{ijk}\eta_{ijk} + \beta_2 \eta_{iik}\eta_{jjk} + \beta_3 \eta_{iik}\eta_{kjj} + \beta_4 \eta_{ijj}\eta_{ikk} + \beta_5 \eta_{ijk}\eta_{kji}, \end{aligned} \tag{20.1}$$

where α_1 and α_2 denote the conventional elastic constants for isotropic materials, $\beta_{1,\ldots,5}$ are the additional material constants accompanied with the five irreducible parts of the strain gradient tensor $\eta_{ijk} = \varepsilon_{kj,i}$ (Lazar, 2016). The formulation of the *modified* strain gradient energy density is derived from MINDLIN's second form

by using the macroscopic vector of rotation $\varphi_i = \frac{1}{2}\epsilon_{ijk}u_{k,j}$, applicable to solids under small deformations. ϵ_{ijk} denotes the LEVI-CIVITA symbol. Taking into account the balance of spin (Abali et al, 2015, 2017), the irreducible parts of η_{ijk} reduce to three. Based on Fleck and Hutchinson (1997), the independent expressions of η_{ijk} are introduced and the second order displacement gradient is decomposed into a symmetric part η^{S}_{ijk} and a remaining part η^{R}_{ijk}. The remaining part is not necessarily anti-symmetric, like the work of Fleck and Hutchinson (1997) supposed, *c.f.* Eq. (20.2). Figure 20.1 shows the scheme of decomposition, where:

$$\begin{aligned}
\eta_{ijk} &= \eta^{\mathrm{S}}_{ijk} + \eta^{\mathrm{R}}_{ijk}\,, \\
\eta^{\mathrm{S}}_{ijk} &= \frac{1}{3}(u_{k,ij} + u_{i,jk} + u_{j,ki})\,, \\
\eta^{\mathrm{R}}_{ijk} &= \frac{2}{3}(\epsilon_{ikl}\bar{\eta}_{lj} + \epsilon_{jkl}\bar{\eta}_{li}) + \epsilon_{kjl}\bar{\eta}_{li}\,.
\end{aligned} \tag{20.2}$$

$\bar{\eta}_{ij} = \varphi_{j,i}$ is the gradient of rotation, which is decomposed into its symmetric and anti-symmetric part, χ^{S}_{ij} and χ^{A}_{ij}, respectively:

$$\chi^{\mathrm{A}}_{ij} = \frac{1}{2}\left(\varphi_{i,j} - \varphi_{j,i}\right), \quad \chi^{\mathrm{S}}_{ij} = \frac{1}{2}\left(\varphi_{i,j} + \varphi_{j,i}\right). \tag{20.3}$$

The tensor η^{S}_{ijk} is further decomposed into its spherical and deviatoric part, $\eta^{(0)}_{ijk}$ and $\eta^{(1)}_{ijk}$, *c.f.*, Fig. 20.1 . The quantity $\eta^{(0)}_{ijk}$ is related to χ^{A}_{ij} and the dilatation gradient $\varepsilon_{mm,i}$ in the following manner:

$$\begin{aligned}
\eta^{(0)}_{ijk} &= \frac{1}{5}\left(\delta_{ij}\eta^{\mathrm{S}}_{mmk} + \delta_{jk}\eta^{\mathrm{S}}_{mmi} + \delta_{ki}\eta^{\mathrm{S}}_{mmj}\right)\,, \\
\eta^{\mathrm{S}}_{mmi} &= \varepsilon_{mm,i} + \frac{2}{3}\epsilon_{iln}\chi^{\mathrm{A}}_{ln}\,, \\
\eta^{(1)}_{ijk} &= \eta^{\mathrm{S}}_{ijk} - \eta^{(0)}_{ijk}\,.
\end{aligned} \tag{20.4}$$

χ^{A}_{ij} is a power conjugated measure for an antisymmetric couple stress tensor. For static problems it can be assumed, that the couple stress tensor μ_{ij} will be symmetric only. Because of that, χ^{A}_{ij} does not influence the strain energy, as it is motivated in Liebold and Müller (2013); Yang et al (2002) and further examined in Münch et al (2015).

Based on Fleck and Hutchinson (1997); Liebold and Müller (2017), the formulation of the modified strain gradient energy density reads:

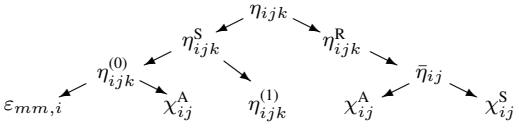

Fig. 20.1 Scheme of decomposition

$$u^{\text{MSG}} = G\varepsilon_{ij}\varepsilon_{ij} + \frac{\lambda}{2}\varepsilon_{kk}\varepsilon_{ii} + G\ell_0^2\varepsilon_{mm,i}\varepsilon_{kk,i} + G\ell_1^2\eta^{(1)}_{ijk}\eta^{(1)}_{ijk} + G\ell_2^2\chi^{\text{S}}_{ij}\chi^{\text{S}}_{ij} \ . \tag{20.5}$$

G and λ are LAMÉ's constants, whereas ℓ_0, ℓ_1 and ℓ_2 denote the three additional material length scale parameters given in the dimension of a length. The multiplication of the higher-order terms by G is arbitrary. The classical strain-energy Eugster and C. (2017) is extended here. Without further reasoning ℓ_0, ℓ_1 and ℓ_2 are set to be equal to ℓ:

$$\boxed{u^{\text{MSG}} = G\varepsilon_{ij}\varepsilon_{ij} + \frac{\lambda}{2}\varepsilon_{kk}\varepsilon_{ii} + G\ell^2\left(\varepsilon_{mm,i}\varepsilon_{kk,i} + \eta^{(1)}_{ijk}\eta^{(1)}_{ijk} + \chi^{\text{S}}_{ij}\chi^{\text{S}}_{ij}\right)} \ . \tag{20.6}$$

The strain and the higher-order strain tensors are:

$$\begin{aligned}
\varepsilon_{ij} &= \frac{1}{2}\left(u_{i,j} + u_{j,i}\right) \ , \\
\chi^{\text{S}}_{ij} &= \frac{1}{4}\left(\epsilon_{ilk}u_{k,lj} + \epsilon_{jlk}u_{k,li}\right) \ , \\
\eta^{(1)}_{ijk} &= \frac{1}{3}(u_{k,ij} + u_{i,jk} + u_{j,ki}) - \frac{1}{15}\big[\delta_{ij}(u_{k,mm} + 2u_{m,mk}) \\
&\quad + \delta_{jk}(u_{i,mm} + 2u_{m,mi}) + \delta_{ki}(u_{j,mm} + 2u_{m,mj})\big] \ ,
\end{aligned} \tag{20.7}$$

given in terms of the displacement field $u_i(\mathbf{x})$.

20.2.2 KIRCHHOFF Plate assumptions

The present work investigates the following restrictions to the displacement field $u_i(\mathbf{x})$ in order to derive the Partial Differential Equation (PDE) of the system and their weak form by the help of variational calculus. The so-called KIRCHHOFF-LOVE model of plates is a two-dimensional mathematical model for thin plates subjected to forces and moments, *c.f.* Fig. 20.2. The assumptions are, that:

- the smallest diameter d is much larger then the thickness t,
- the mid-surface plane is the only deformation plane,
- forces are prependicular to the deformation plane,
- straight lines normal to the mid-surface remain straight and normal after deformation,
- the thickness of the plate does not change during the deformation
- the deformations are small.

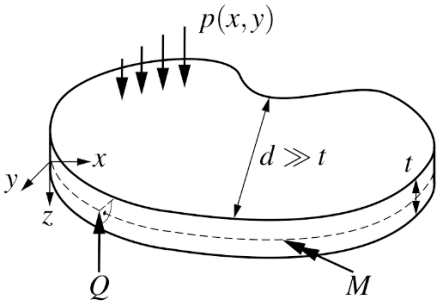

Fig. 20.2 Outline of a KIRCHHOFF-LOVE plate

The displacement field of a KIRCHHOFF-LOVE plate reads:

$$u_x = -z\frac{\partial w(x,y)}{\partial x}\ , \quad u_y = -z\frac{\partial w(x,y)}{\partial y}\ , \quad u_z = w(x,y) \tag{20.8}$$

where $w(x,y)$ is the bending plane, $p(x,y)$ the load distribution, Q the boundary force and M the boundary moment.

20.2.3 Variation of the Modified Strain Energy of a KIRCHHOFF Plate

The strain energy density of the problem is derived by evaluating the prescribed displacement field Eq. (20.8) in combination with u^{MSG}, Eq. (20.6). Partial derivatives are denoted by subscripts in the following manner:

$$\frac{\partial(\cdot)}{\partial x} = (\cdot)_x\ , \quad \frac{\partial(\cdot)}{\partial y} = (\cdot)_y\ , \quad \frac{\partial^2(\cdot)}{\partial x \partial y} = (\cdot)_{xy}\ . \tag{20.9}$$

The first term in Eq. (20.6) becomes

$$\varepsilon_{ij}\varepsilon_{ij} = (zw_{xx})^2 + 2\,(zw_{xy})^2 + (zw_{yy})^2\ , \tag{20.10}$$

the second one

$$\varepsilon_{kk}\varepsilon_{ii} = (zw_{xx})^2 + 2z^2 w_{xx}w_{yy} + (zw_{yy})^2\ , \tag{20.11}$$

the third one

$$\begin{aligned}\varepsilon_{mm,i}\varepsilon_{kk,i} = {} & (zw_{xxx})^2 + (zw_{yyy})^2 + (zw_{yyx})^2 + (zw_{xxy})^2 + \\ & + 2\,(zw_{xxx})\,(zw_{yyx}) + 2\,(zw_{xxy})\,(zw_{yyy}) + 2w_{xx}w_{yy} + \\ & + w_{xx}^2 + w_{yy}^2\ ,\end{aligned} \tag{20.12}$$

the fourth one

$$\eta^{(1)}_{ijk}\eta^{(1)}_{ijk} = \frac{2}{5}\left(zw_{xxx}\right)^2 + \frac{2}{5}\left(zw_{yyy}\right)^2 + \frac{12}{5}\left(zw_{yyx}\right)^2 + \frac{12}{5}\left(zw_{xxy}\right)^2 - \frac{6}{5}zw_{xxx}\,zw_{yyx} - \frac{6}{5}zw_{yyy}\,zw_{xxy} + \frac{4}{15}w^2_{xx} + + \frac{4}{15}w^2_{yy} - \frac{2}{15}w_{xx}w_{yy} + \frac{2}{3}w^2_{yy}\,, \tag{20.13}$$

and the last one

$$\chi^{\mathrm{S}}_{ij}\chi^{\mathrm{S}}_{ij} = \frac{1}{2}\left(w_{xx} + w_{yy}\right)^2\ . \tag{20.14}$$

In summary, the modified strain energy density is:

$$\begin{aligned} u^{\mathrm{MSG}} &= \frac{7}{5}G\ell^2z^2\left[w^2_{xxx} + w^2_{yyy}\right] + \frac{17}{5}G\ell^2z^2\left[w^2_{yyx} + w^2_{xxy}\right] \\ &+ \frac{4}{5}G\ell^2z^2\left[w_{xxx}\,w_{yyx} + w_{xxy}\,w_{yyy}\right] \\ &+ \left(Gz^2 + \frac{\lambda}{2}z^2 + \frac{53}{30}G\ell^2\right)\left[w^2_{xx} + w^2_{yy}\right] \\ &+ \left(z^2\lambda + \frac{13}{5}G\ell^2\right)w_{xx}\,w_{yy} + \left(2Gz^2 + \frac{2}{3}G\ell^2\right)w^2_{yx}\,. \end{aligned} \tag{20.15}$$

For a proof of concept, this work restricts to a square plate of the length L and of thickness t. Then, the variation of the strain energy is derived as follows:

$$\begin{aligned} \delta W^{\mathrm{MSG}} &= \int_V \delta u^{\mathrm{MSG}}\,\mathrm{d}V \\ &= \int_{-\frac{t}{2}}^{+\frac{t}{2}}\int_0^L\int_0^L \Bigg(\frac{14}{5}G\ell^2z^2\left[w_{xxx}\delta w_{xxx} + w_{yyy}\delta w_{yyy}\right] \\ &+ \frac{34}{5}G\ell^2z^2\left[w_{yyx}\delta w_{yyx} + w_{xxy}\delta w_{xxy}\right] \\ &+ \frac{4}{5}G\ell^2z^2\left[\delta w_{xxx}\,w_{yyx} + w_{xxx}\,\delta w_{yyx} + \delta w_{xxy}\,w_{yyy} + w_{xxy}\,\delta w_{yyy}\right] \\ &+ \left(2Gz^2 + \lambda z^2 + \frac{53}{15}G\ell^2\right)\left[w_{xx}\delta w_{xx} + w_{yy}\delta w_{yy}\right] \\ &+ \left(z^2\lambda + \frac{13}{5}G\ell^2\right)\left[\delta w_{xx}\,w_{yy} + w_{xx}\,\delta w_{yy}\right] \\ &+ \left(4Gz^2 + \frac{4}{3}G\ell^2\right)w_{yx}\delta w_{yx}\Bigg)\,\mathrm{d}x\mathrm{d}y\mathrm{d}z\,. \end{aligned} \tag{20.16}$$

Employing the rules of variational calculus and multiple application of two-dimensional partial integration, δW^{MSG} becomes:

$$\begin{aligned}\delta W^{\mathrm{MSG}} = -\frac{t^3}{12}\int_0^L\int_0^L \delta w\Bigg[&\frac{14}{5}G\ell^2\left(w_{xxxxxx}+w_{yyyyyy}\right)\\ &+\frac{42}{5}G\ell^2\left(w_{xxxxyy}+w_{yyyyxx}\right)\\ &-\left(2G+\lambda+\frac{212}{5}G\frac{\ell^2}{t^2}\right)\left(w_{xxxx}+w_{yyyy}+2w_{xxyy}\right)\Bigg]\mathrm{d}x\mathrm{d}y\\ &+\frac{Gt^3}{12}\int_0^L \Lambda_1(x,y)\Big|_{y=0}^{y=L}\mathrm{d}x+\frac{Gt^3}{12}\int_0^L \Lambda_2(x,y)\Big|_{x=0}^{x=L}\mathrm{d}y\,,\end{aligned} \tag{20.17}$$

with Λ_1 and Λ_2 being the boundary relations:

$$\begin{aligned}\Lambda_1(x,y) = &\left(\frac{7}{5}\ell^2 w_{yyy}+\frac{2}{5}\ell^2 w_{xxy}\right)\delta w_{yy}+\left(\frac{17}{5}\ell^2 w_{xxy}+\frac{2}{5}\ell^2 w_{yyy}\right)\delta w_{xx}\\ &+\Bigg[\left(\frac{\lambda}{G}+\frac{78}{5}\frac{\ell^2}{t^2}\right)w_{xx}+\left(1+\frac{\lambda}{2G}+\frac{106}{5}\frac{\ell^2}{t^2}\right)w_{yy}-\frac{7}{5}\ell^2 w_{yyyy}\\ &-\frac{17}{5}\ell^2 w_{yyxx}-\frac{2}{5}\ell^2\left(w_{xxxx}+w_{xxyy}\right)\Bigg]\delta w_y+\left(1+4\frac{\ell^2}{t^2}\right)w_{xy}\,\delta w_x\\ &+\Bigg[\frac{7}{5}\ell^2 w_{yyyyy}+\frac{17}{5}\ell^2 w_{yyyxx}+\frac{2}{5}\ell^2\left(w_{xxxxy}+w_{xxyyy}\right)\\ &-\left(\frac{\lambda}{G}+\frac{78}{5}\frac{\ell^2}{t^2}\right)w_{xxy}\\ &-\left(1+\frac{\lambda}{2G}+\frac{106}{5}\frac{\ell^2}{t^2}\right)w_{yyy}-\left(1+4\frac{\ell^2}{t^2}\right)w_{yxx}\Bigg]\delta w\,,\end{aligned} \tag{20.18}$$

and

$$\begin{aligned}\Lambda_2(x,y) = &\left(\frac{7}{5}\ell^2 w_{xxx}+\frac{2}{5}\ell^2 w_{yyx}\right)\delta w_{xx}+\left(\frac{17}{5}\ell^2 w_{yyx}+\frac{2}{5}\ell^2 w_{xxx}\right)\delta w_{yy}\\ &+\Bigg[\left(\frac{\lambda}{G}+\frac{78}{5}\frac{\ell^2}{t^2}\right)w_{yy}+\left(1+\frac{\lambda}{2G}+\frac{106}{5}\frac{\ell^2}{t^2}\right)w_{xx}-\frac{7}{5}\ell^2 w_{xxxx}\\ &-\frac{17}{5}\ell^2 w_{yyxx}-\frac{2}{5}\ell^2\left(w_{xxxx}+w_{xxyy}\right)\Bigg]\delta w_y+\left(1+4\frac{\ell^2}{t^2}\right)w_{xy}\,\delta w_x\\ &+\Bigg[\frac{7}{5}\ell^2 w_{xxxxx}+\frac{17}{5}\ell^2 w_{xxxyy}+\frac{2}{5}\ell^2\left(w_{yyyyx}+w_{yyxxx}\right)\\ &-\left(\frac{\lambda}{G}+\frac{78}{5}\frac{\ell^2}{t^2}\right)w_{yyx}-\left(1+\frac{\lambda}{2G}+\frac{106}{5}\frac{\ell^2}{t^2}\right)w_{xxx}\\ &-\left(1+4\frac{\ell^2}{t^2}\right)w_{xyy}\Bigg]\delta w\,.\end{aligned} \tag{20.19}$$

In fact, the formulations Λ_1 and Λ_2 at the boundaries would allow to identify boundary-forces and -moments, when considering the work done by the external loads. In the present work, the external loads are limited to the application of a pressure distribution $p(x,y)$.

20.2.4 The Governing Tri-harmonic Plate Equation

To derive the respective partial differential equation for static problems, the difference of the virtual strain energy and the virtual work done by the external loads δA, assumed as:

$$\begin{aligned}\delta A = &\int_0^L \int_0^L p(x,y)\delta w \,\mathrm{d}x\,\mathrm{d}y \\ &+ \int_0^L \Big[Q\delta w - M^y \delta w_x - M^x \delta w_y + M^{Hy}\delta w_{xx} + M^{Hx}\delta w_{yy} \Big]_{x=0}^{x=L} \mathrm{d}x \\ &+ \int_0^L \Big[Q\delta w - M^y \delta w_x - M^x \delta w_y + M^{Hy}\delta w_{xx} + M^{Hx}\delta w_{yy} \Big]_{x=0}^{x=L} \mathrm{d}y \,,\end{aligned} \tag{20.20}$$

has to be minimized, where M^x and M^y are classical moments, which affect the deflection angle (first derivative) of w at the boundaries. M^{Hx} and M^{Hy} are higher order moments, affecting the curvature (second derivative) in the respective direction at the boundaries. An energy minimization yields in:

$$\delta W^{\mathrm{MSG}} - \delta A = \delta \Pi \,, \quad \delta \Pi \to 0 \qquad \Rightarrow \qquad \delta W^{\mathrm{MSG}} = \delta A \,, \tag{20.21}$$

and by comparison of Eq. (20.17) and (20.20) the *tri-harmonic plate equation* arises:

$$\boxed{D\Delta\Delta w(x,y) - H\Delta\Delta\Delta w(x,y) = p(x,y)} \,, \tag{20.22}$$

using the Laplacian $\Delta(\cdot) = (\cdot)_{xx} + (\cdot)_{yy}$. Similarities can be drawn to the result of Kotchergenko (2015). In the present work, the plate stiffnesses are:

$$D = \frac{t^3}{12}\left(2G + \lambda + \frac{212}{5} G \frac{\ell^2}{t^2}\right) \,, \quad H = \frac{7}{60} G t^3 \ell^2 \,. \tag{20.23}$$

In the limit case to the conventional continuum theory, if $\ell = 0$, Eq. (20.22) will turn into the classical Kirchhoff plate equation.

20.2.5 A NAVIER-Solution with FOURIER-Series

Combining the continuous ansatz for *simply supported rectangular plates* after NAVIER (Becker and Gross, 2002):

$$w_{\text{ana}}^{\text{SG}}(x,y) = \sum_{m=1}^{\infty}\sum_{n=1}^{\infty} w_{mn} \sin\left(\frac{m\pi x}{L}\right) \sin\left(\frac{n\pi y}{L}\right) \tag{20.24}$$

and rewriting the load-function as follows:

$$p(x,y) = \sum_{m=1}^{\infty}\sum_{n=1}^{\infty} p_{mn} \sin\left(\frac{m\pi x}{L}\right) \sin\left(\frac{n\pi y}{L}\right) \ , \tag{20.25}$$

$$p_{mn} = \frac{4}{L^2}\int_0^L\int_0^L p(x,y) \sin\left(\frac{m\pi x}{L}\right) \sin\left(\frac{n\pi y}{L}\right) \mathrm{d}x\mathrm{d}y \ , \tag{20.26}$$

a solution for the equation (20.22) is given in form of a series in Eq. (20.24), having the coefficients:

$$\begin{aligned} w_{mn} = p_{mn}\Big\{ & D\left[\left(\frac{m\pi}{L}\right)^4 + \left(\frac{n\pi}{L}\right)^4 + 2\left(\frac{n\pi}{L}\right)^2\left(\frac{m\pi}{L}\right)^2\right] \\ & + H\left[\left(\frac{m\pi}{L}\right)^6 + \left(\frac{n\pi}{L}\right)^6 + 3\left(\frac{m\pi}{L}\right)^4\left(\frac{n\pi}{L}\right)^2 + 3\left(\frac{m\pi}{L}\right)^2\left(\frac{n\pi}{L}\right)^4\right]\Big\}^{-1} . \end{aligned} \tag{20.27}$$

For a constant distribution of loads $p(x,y)$, a sufficient convergence of this series is achieved by taking about 50 terms into account for m and n.

20.3 A C^1– continuous Finite Element Approach

20.3.1 The Weak Form of the PDE

The weak form of the tri-harmonic plate equation, Eq. (20.22), is in a sense already given with the variation of the strain gradient energy density in Eq. (20.16), only by replacing the variational terms by the independent test-functions $v(x,y)$:

$$
\begin{aligned}
&\overbrace{\qquad\qquad\qquad\qquad\qquad\qquad}^{f(v)}\\
&\int_V p(x,y)\, v(x,y)\mathrm{d}V\\
&= \int_V \frac{14}{5}G\ell^2 z^2\left[w_{xxx}v_{xxx} + w_{yyy}v_{yyy}\right] + \frac{34}{5}G\ell^2 z^2\left[w_{yyx}v_{yyx} + w_{xxy}v_{xxy}\right]\\
&\quad + \frac{4}{5}G\ell^2 z^2\left[v_{xxx}\, w_{yyx} + w_{xxx}\, v_{yyx} + v_{xxy}\, w_{yyy} + w_{xxy}\, v_{yyy}\right]\\
&\quad + \left(2Gz^2 + \lambda z^2 + \frac{53}{15}G\ell^2\right)\left[w_{xx}v_{xx} + w_{yy}v_{yy}\right]\\
&\quad + \left(z^2\lambda + \frac{13}{5}G\ell^2\right)\left[v_{xx}\, w_{yy} + w_{xx}\, v_{yy}\right] + \left(4Gz^2 + \frac{4}{3}G\ell^2\right) w_{yx}v_{yx}\mathrm{d}V\\
&\underbrace{\qquad\qquad\qquad\qquad\qquad\qquad}_{a(v,w)}
\end{aligned}
\tag{20.28}
$$

The left-hand side is the so-called bi-linear form $a(v, w)$ of the PDE. The right-hand side $f(v)$ is formed, using the variation of the work done by external loads (Eq. 20.20) with the same replacement. It can be seen, that the weak form is only a third-order partial differential equation in both, the test- and trial-functions, $v(x, y)$ and $w(x, y)$.

20.3.2 Two Dimensional Hermite Finite Element Formulation

The requirements for a straight-forward finite element solution for the present weak form are: (i), that the basis functions for the Galerkin discretization are at least three times differentiable and (ii), that the global behavior of the solution fulfills C^1–continuity. The latter is needed due to the fact, that the strain energy used in Eq. (20.6) evaluates second derivatives of displacements and in the end of the test- and trial-functions, too. To guarantee, that the second derivatives in each element will be well connected to the global behavior, the first derivatives need to be continuous inbetween the neighboring elements. Both requirements are fulfilled using so-called Hermite finite element formulations, which consist of the Hermite polynomials, as plotted in Fig. (20.3):

$$
\begin{aligned}
H_1(\zeta) &= 2\zeta^3 - 3\zeta^2 + 1\,, \qquad & H_2(\zeta) &= \zeta^3 - 2\zeta^2 + \zeta\,,\\
H_3(\zeta) &= -2\zeta^3 + 3\zeta^2\,, & H_4(\zeta) &= \zeta^3 - \zeta^2,
\end{aligned}
\tag{20.29}
$$

which are linearly superposed and multiplicatively connected to form either 1D or 2D test- and trail-functions v^{e} and w^{e} per element, e,

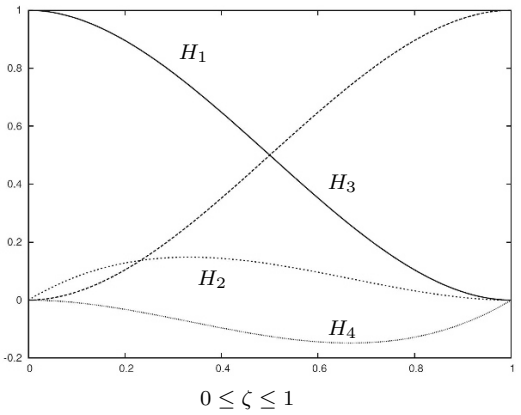

Fig. 20.3 Plot of the HERMITE polynomials

$$v^{\mathrm{e}}(\zeta,\xi) = \sum_{\alpha=1}^{4}\sum_{\beta=1}^{4} H_\alpha(\zeta) H_\beta(\xi)\ , \quad w^{\mathrm{e}}(\zeta,\xi) = \sum_{\delta=1}^{4}\sum_{\gamma=1}^{4} c^{\mathrm{e}}_{\delta\gamma} H_\delta(\zeta) H_\gamma(\xi)\ , \tag{20.30}$$

where $c^{\mathrm{e}}_{\delta\gamma}$ denote the coefficients (the unknowns) to be calculated to form the solution. Such element formulations are called BOGNER–FOX–SCHMIT elements Bogner et al (1965). Two exemplary combinations $\Phi_1 = H_1 H_1$ and $\Phi_2 = H_1 H_2$ are given in Fig. (20.4). Φ_1 will directly influence the value of deflection at the node position (0,0), whereas Φ_2 will influence the first derivative in the ζ-direction. Equation (20.30) is used in the following condensed form:

$$v^{\mathrm{e}}(\zeta,\xi) = \sum_{i=1}^{16} \Phi_i(\zeta,\xi)\ , \quad w^{\mathrm{e}}(\zeta,\xi) = \sum_{i=1}^{16} c^{\mathrm{e}}_i \Phi_i(\zeta,\xi)\ , \tag{20.31}$$

where the assignment of the combinations for $\Phi_i \to H_\alpha H_\beta$ is: $(i \to \alpha\beta)$ $1 \to 11$, $2 \to 12$, $3 \to 13$, $4 \to 14$, $5 \to 21$, $6 \to 22$, $7 \to 23$, $8 \to 24$, $9 \to 31$, $10 \to 32$, $11 \to 33$, $12 \to 34$, $13 \to 41$, $14 \to 42$, $15 \to 43$ and $16 \to 44$. c^{e}_i represent the 16 coefficients per element, of which four of them directly represent the value of deflections at the four nodes, eight of them represent the first derivatives

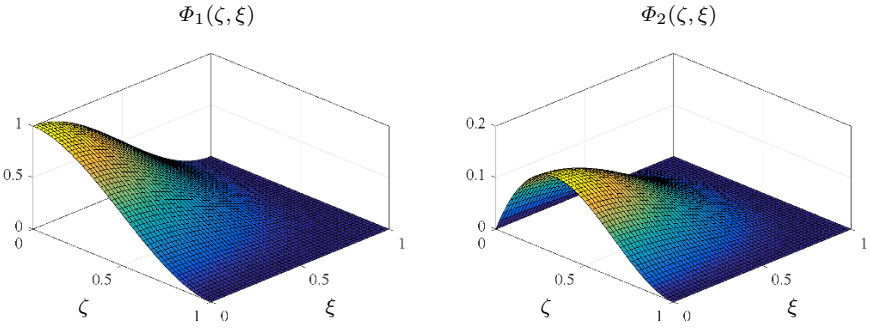

Fig. 20.4 Exemplary two-dimensional HERMITE polynomials acting on the node (0,0)

in each direction at the nodes and four of them carry the information of the so-called internal- (or bubble-) modes.

20.3.3 The Element and Global Stiffness Matrix and Realization of the Boundary Condition

The element stiffness matrix is established by inserting the test- and trial-functions into the integral weak form. Doing so, Eq. (20.28) is rewritten:

$$\mathbf{K}^{\mathrm{e}}\mathbf{c}^{\mathrm{e}} = \mathbf{f}^{\mathrm{e}} , \qquad \mathbf{c}^{\mathrm{e}} = [c_1^{\mathrm{e}},\ c_2^{\mathrm{e}},\ \ldots, c_{16}^{\mathrm{e}}\ ]^{\mathrm{T}} , \tag{20.32}$$

such that the left-hand side is represented by $\mathbf{K}^{\mathrm{e}}\mathbf{c}^{\mathrm{e}}$, with $\mathbf{K}^{\mathrm{e}}$ being the element stiffness matrix and $\mathbf{c}^{\mathrm{e}}$ the vector of coefficients, and the right-hand side is expressed by thev vector $\mathbf{f}^{\mathrm{e}}$. Using the element stiffness components:

$$K_{i|j}^{\mathrm{e}} = a^{\mathrm{e}}(\Phi_i, \Phi_j) , \tag{20.33}$$

in which a^{e} denotes the bilinearform in the integration domain of a single element, the weak form Eq. (20.28) per element can be expressed as:

$$\begin{bmatrix} K_{1|1}^{\mathrm{e}} & K_{1|2}^{\mathrm{e}} & \cdots & K_{1|16}^{\mathrm{e}} \\ K_{2|1}^{\mathrm{e}} & K_{2|2}^{\mathrm{e}} & \cdots & K_{2|16}^{\mathrm{e}} \\ \vdots & \vdots & \ddots & \vdots \\ K_{16|1}^{\mathrm{e}} & K_{16|2}^{\mathrm{e}} & \cdots & K_{16|16}^{\mathrm{e}} \end{bmatrix} \begin{bmatrix} c_1^{\mathrm{e}} \\ c_2^{\mathrm{e}} \\ \vdots \\ c_{16}^{\mathrm{e}} \end{bmatrix} = \begin{bmatrix} \int_{V^{\mathrm{e}}} p(\zeta,\xi)\, \Phi_1 \, \mathrm{d}V^{\mathrm{e}} \\ \int_{V^{\mathrm{e}}} p(\zeta,\xi)\, \Phi_2 \, \mathrm{d}V^{\mathrm{e}} \\ \vdots \\ \int_{V^{\mathrm{e}}} p(\zeta,\xi)\, \Phi_{16} \, \mathrm{d}V^{\mathrm{e}} \end{bmatrix} . \tag{20.34}$$

In a next step the global stiffness matrix is developed. To achieve a sparse band matrix, which will have advantages in dissolving large systems, the lexicographical distribution of nodes is used here, *c.f.* Fig. (20.5). Here, the nodes at the physi-

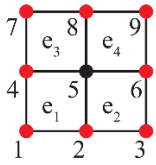

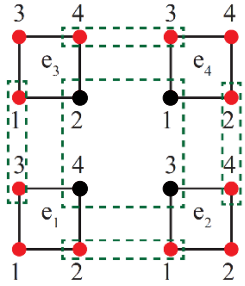

Fig. 20.5 Left: the lexicographical distribution of nodes; right: the numbering of nodes per element $\mathrm{e_N}$ for a minimal discretization of a plate

cal boundary of the plate are highlighted to be remembered for the assignement of Dirichlet boundary conditions, whereas node number "5" is used to demonstrate,

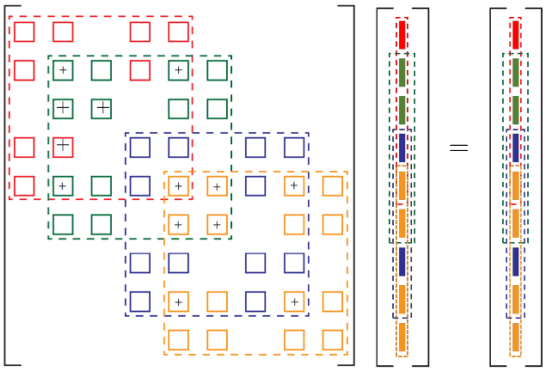

Fig. 20.6 Scheme of the composition of the global matrix equation

that its value of deflection as well as the derivatives belong to all four neighboring elements at the same time. This is achieved by assembling the global stiffness matrix by overlapping the element matrices in this way, such that the respective values of deflection as well as the derivatives are multiplied with the same coefficients c, respectively. Therefor, the element's matrices are split into 4×4 submatrices, in which the components will represent the deflection, the derivatives and the internal mode for a single node of an element. Figure (20.6) demontrates the scheme of composition of the global system of equations. This scheme represents the global linear algebraic equation:

$$\mathbf{K}^{\mathrm{G}}\mathbf{c}^{\mathrm{G}} = \mathbf{f}^{\mathrm{G}} , \tag{20.35}$$

where the dashed lines in Fig. (20.6) declare an assignment to single elements and squares to the 4×4 submatrices. The DIRICHLET boundary condition for a simply supported plate is realized by a direct manipulation of the coefficients of the respective boundary nodes. For the reason that the deflection at the boundary nodes are set equal to zero, the respective columns are removed in the global stiffness matrix. The reduced system of equations, denoted by the superscript S, is solved with the *backslash* operator of `Matlab` (MathWorks, Inc.):

$$\mathbf{c}^{\mathrm{S}} = \mathbf{K}^{\mathrm{S}} \backslash \mathbf{f}^{\mathrm{S}} , \tag{20.36}$$

using a banded solver. The procedure described here is numerically rather fast and in general applicable to different situations or geometries.

20.4 Results

For the numerical simulations and tests for convergence and size effect, a squared micro-plate of the length L and thickness t is used. Figure (20.7) represents the deflection of the plate, which is simply supported at all edges and loaded by the constant distribution of force $p(x, y)$. Table 20.1 gives the material and geometry

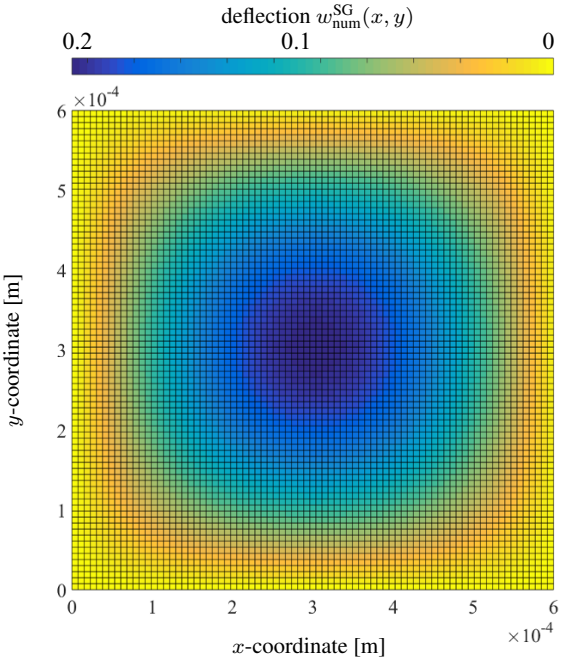

Fig. 20.7 Deflection of the midplane of a square plate, $t = 30\,\mu\text{m}$, $L = 20t$, $\ell = 10\,\mu\text{m}$, NumOfEl=6400

parameters, which are quite realistic when modeling a small polymer plate (Chong, 2002; Kong et al, 2009; Lam et al, 2003; Nikolov et al, 2007). $w^{SG}_{num}(x,y)$ denotes the numerical result of the deflection of the plate at the coordinate x and y w.r.t. the Second Gradient (SG) continuum approach, whereas w^{SG}_{ana} denotes the "'analytical result"' from the truncated FOURIER-series, *c.f.* Eq. (20.24). $w^{class}(x,y)$ will represent the solution of plate-bending for the classical CAUCHY-continuum theory. Figure (20.8) shows the behavior of the numerical solution of the midpoint of the plate while refining the mesh of elements.

20.4.1 Concerning the Convergence

To demonstrate the convergence behavior of the present numerical approach, solutions with different sizes of equidistantly distrubuted elements were conducted. The global number of degrees of freedoms (DOF) is used to compare different solutions.

Table 20.1 Thickness t, lengths L, elastic modulus E, material length scale parameter ℓ and the distributed load $p(x,y)$ used for the plate simulations

t	L	E	ℓ	$p(x,y)$
$30\,\mu\text{m}$	$20\,t$	$3.8\,\text{GPa}$	$10\,\mu\text{m}$	$10\,\text{MPa}$

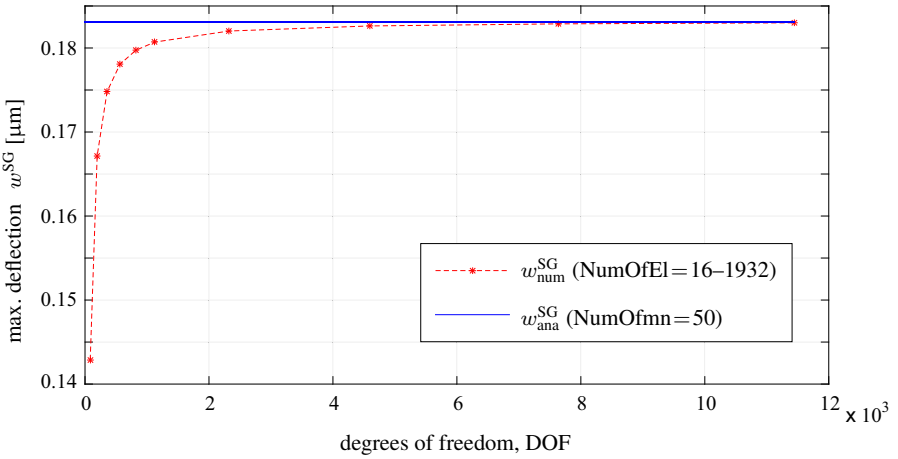

Fig. 20.8 Convergence of the deflections of the center point compared to the analytical value for $t = 30\,\mu\text{m}$

For the beginning, Fig. (20.8) gives the absolute deflection of the center point $(\frac{L}{2}, \frac{L}{2})$ of the plate for different mesh sizes, in comparison to the constant analytical value.

It has to be remarked, that with the same set of parameters used in Fig. (20.8), the classical value (where ℓ is equal to zero) is more than twice as large as the second gradient (SG) solution. In a next investigation, in Fig. (20.9), the error in percent between the numerical and the FOURIER solution is charted for different degrees of freedom. The error between the numerical and the analytical values for the deflection of the center point is calculated by:

$$\text{error} = \left| \frac{w^{SG}_{num}}{w^{SG}_{ana}} - 1 \right| \times 100\,. \tag{20.37}$$

In the logarithmic plot of the error we clearly observe a quite constant rate of convergence. From a certain number of degrees of freedom on, the convergence rate seems to increase. In the authors opinion, this fact is due to the truncation of the FOURIER solution at m=50, which is taken as the reference value. It can be assumed, that the numerical solution passes the truncated FOURIER solution at a further point of DOFs. Beside this assumption, it has to be taken into account, that the computational errors, which go along with these very large numbers of calculation steps, will add up and will shift the solution for very large DOFs. In summary, however, from a numerical point of view, the approach shown is extremely robust and well-built, reaching an error of $0.1\,\%$ quite easily.

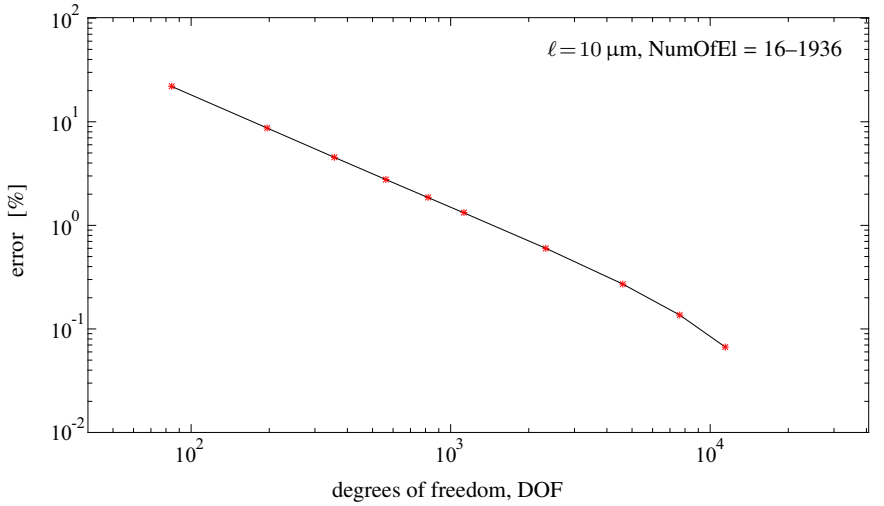

Fig. 20.9 Convergence of the error between numerical and analytical deflections of the midpoint for $t = 30$ µm in a logarithmic plot

20.4.2 Results for the Size Effect

For the analysis of the size dependent behavior of the solutions, the ratio of both – the numerical as well as the FOURIER solution – to the result of the classical continuum theory (without any length scale influence) is calculated for different sizes of the plate, *c. f.* Fig. (20.10). The ratio of the length to the thickness is constant. The numerical values in Fig. (20.10) are calculated for a more or less coarse mesh using 16 elements, which includes a constant error of about 21 %.

20.4.3 Analysis of the C^1–continuity

To demonstrate the intended C^1–continuity of the present solution, a cascade of results along a center line $(x, \frac{L}{2})$ is established: (i) for the z-deflections, see Fig. (20.11), (ii) the first derivatives in the x-direction, see Fig. (20.12) an (iii) the second derivatives in the x-direction, see Fig. (20.13).

The plots in Figs. (20.11–20.13) are based on the post-prozessed data for the element's solutions. In each interval, the slope of the weighted HERMITE element function, Eq. $(20.30)_2$, is plotted independently. The element's solutions for the 0^{th} and 1^{st} derivatives are continuously connected between the elements. The first derivative at a node of one element equals the first derivative of the neighbouring element, and so on. A different picture is drawn, when looking at the second derivatives. Fig. (20.13) demonstrates by the jumps between the element solutions, that the sec-

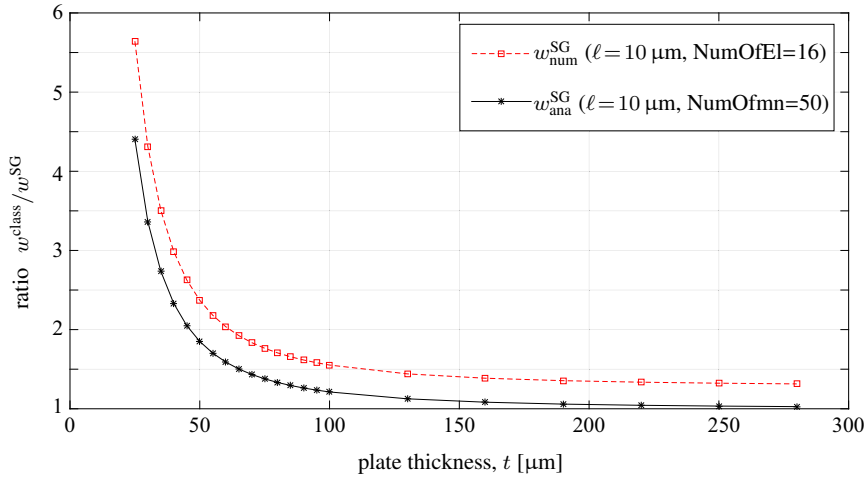

Fig. 20.10 Size effect for a square plate, $L = 20t$; numerical vs. analytical results of the deflection of the midpoint $w^{SG}(\frac{L}{2}, \frac{L}{2})$ in relation to the classical result w^{class}

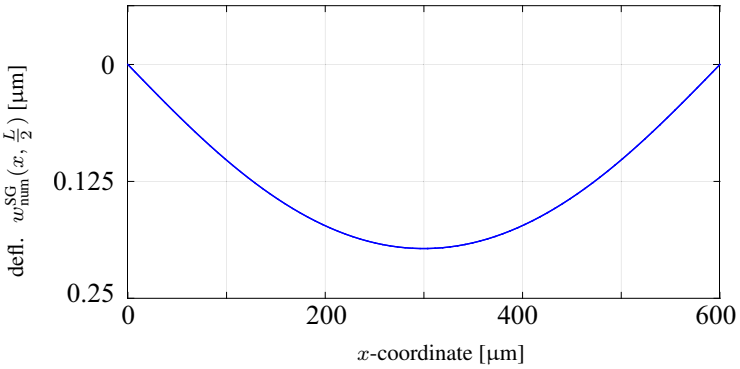

Fig. 20.11 Deflection of the center line of a square plate, $t = 30$ µm, $L = 20t$, $\ell = 10$ µm, NumOfEl = 80×80

ond derivative at a node of one element does not equal the second derivative of the neighbouring element. This behavior of the numerical solution suggests, that the intended C^1–continuity is fulfilled.

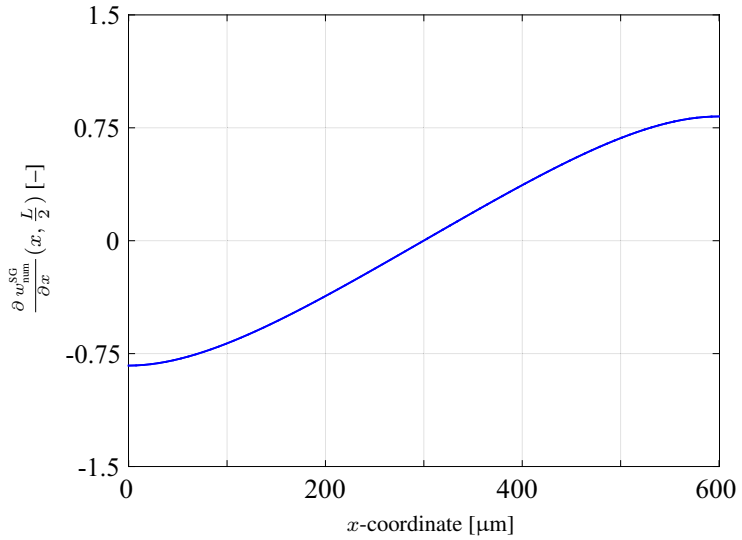

Fig. 20.12 First derivative of the deflection of the center line, $t = 30\,\mu\mathrm{m}$, $L = 20t$, $\ell = 10\,\mu\mathrm{m}$, NumOfEl = 80×80

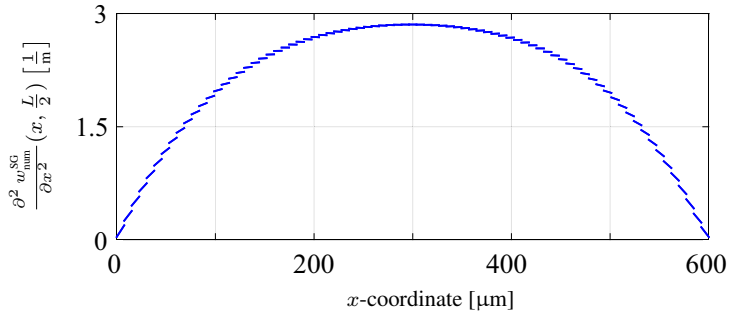

Fig. 20.13 Second derivative of the deflection of the center line, $t = 30\,\mu\mathrm{m}$, $L = 20t$, $\ell = 10\,\mu\mathrm{m}$, NumOfEl = 80×80

20.5 Conclusions

A modified second gradient continuum theory of elasticity was elaborated. The restriction on the displacement field of a Kirchhoff-Love plate was carried out in order to derive the corresponding partial differential equation (the *tri-harmonic equation*) and its weak form, respectively. In order to keep the first derivative of the solution continuous, the problem was discretized using Hermite polynomials, of which the so-called Bogner–Fox–Schmit elements consist of. So far, the present resluts are restricted to equidistantly distributed quad element meshes. It is further accom-

panied by a large number of element coefficients in comparison to a conventional FEM. The elaborated FE approximations show a size effect, as expected from the higher-order theory, as well as convergence in terms of increasing degrees of freedoms in the mesh discretization. This will allow to simulate the elastostatic problem of Kirchhoff-Love plates in arbitrary geometries for micromechanical applications, when considering a higher-order material behavior.

References

Abali BE, Müller WH, Eremeyev VA (2015) Strain gradient elasticity with geometric nonlinearities and its computational evaluation. Mechanics of Advanced Materials and Modern Processes 1(4):2–11

Abali BE, Müller WH, dell'Isola F (2017) Theory and computation of higher gradient elasticity theories based on action principles. Archive of Applied Mechanics 87(9):1495–1510, DOI 10.1007/s00419-017-1266-5

Becker W, Gross D (2002) Mechanik elastischer Körper und Strukturen. Springer-Verlag, Berlin Heidelberg

Bogner FK, Fox RL, A SL (1965) The generation of interelement compatible stiffness and mass matrices by the use of interpolation formulas. In: Proceedings of the Conference on Matrix Methods in Structural Mechanics, Wright-Patterson Air Force Base, Ohio, pp 397–444

Chong CM (2002) Experimental investigation and modeling of size effect in elasticity. PhD thesis, Hong Kong University of Science and Technology

Cuenot S, Fretigny C, Demoustier-Champagne S, Nysten B (2004) Surface tension effect on the mechanical properties of nanomaterials measured by atomic force microscopy. Physical Review B 69:01–05

Eremeyev VA, dell'Isola F (2018) A note on reduced strain gradient elasticity. Generalized Models and Non-classical Approaches in Complex Materials 1:301–310

Eugster SR, C G (2017) On the notion of stress in classical continuum mechanics. Mathematics and Mechanics of Complex Materials 5

Fleck NA, Hutchinson JW (1997) Strain gradient plasticity. In: W HJ, Y WT (eds) Advances in Applied Mechanics, Academic Press, New York, pp 295–361

Giorgio I, dell'Isola F, Steigmann DJ (2018) Axisymmetric deformations of a 2nd grade elastic cylinder. Mechanics Research Communications 94:45–48

Kong S, Zhou S, Nie Z, Wang K (2009) Static and dynamic analysis of micro beams based on strain gradient elasticity theory. International Journal of Engineering Science 47:487–498

Kotchergenko ID (2015) The tri-harmonic plate bending equation. WIT Transactions on Modelling and Simulation 59:367–378

Lam DCC, Yang F, Chong CM, Wang J, Tong P (2003) Experiments and theory in strain gradient elasticity. J Mech Phys Sol 51(8):1477–1508

Lazar M (2016) Irreducible decomposition of strain gradient tensor in isotropic strain gradient elasticity. ZAMM - Journal of Applied Mathematics and Mechanics / Zeitschrift für Angewandte Mathematik und Mechanik 96(11):1291–1305

Li XF, Wang BL, Lee KY (2010) Size effect in the mechanical response of nanobeams. J of Adv Research in Mech Eng 1(1):4–16

Liebold C, Müller WH (2013) Measuring material coefficients of higher gradient elasticity by using AFM techniques and Raman-spectroscopy. In: Altenbach H, Forest S, Krivtsov A (eds) Generalized continua as models for materials, Advanced Structured Materials, 22, pp 255–271

Liebold C, Müller WH (2017) 1D Hermite elements for C1–continuous solutions in second gradient elasticity. Acta Polytechnica CTU Proceedings 7:33–37

McFarland AW, Colton JS (2005) Role of material microstructure in plate stiffness with relevance to microcantilever sensors. Journal of Micromechanics and Microengineering 15(5):1060–1067
Mindlin RD, Tiersten HF (1962) Effects of couple-stresses in linear elasticity. ARMA 11:415–448
Münch I, Neff P, Madeo A, Ghiba ID (2015) The modified indeterminate couple stress model: Why yang et al.'s arguments motivating a symmetric couple stress tensor contain a gap and why the couple stress tensor may be chosen symmetric nevertheless. preprint, arXiv, 1512.02053
Nikolov S, Han CS, Raabe D (2007) On the origin of size effects in small-strain elasticity of solid polymers. International Journal of Solids and Structures 44:1582–1592
Toupin RA (1962) Elastic materials with couple-stresses. ARMA 11:385–414
Yang F, Chong CM, Lam DCC, Tong P (2002) Couple stress based strain gradient theory for elasticity. International Journal of Solids and Structures 39(10):2731–2743